Volume 1 | Number 1 | Jan 2013 | Pages 1–100

ROYAL SOCIETY OF CHEMISTRY

ROYAL SOCIETY OF CHEMISTRY

www.rsc.org/advances

RSC Advances

ARTICLE

Direct Oxidation of Methane to Methanol on Fe–O Modified Graphene

Sarawoot Impeng[a,b], Pipat Khongpracha[a,b], Chompunuch Warakulwit[a,b], Bavornpon Jansang[c], Jakkapan Sirijaraensre[a,b], Masahiro Ehara[d] and Jumras Limtrakul[a,b,e*]

Introduction of functional groups to graphene can be used for the rational design of catalysts for the oxidation of hydrocarbons to alcohols. We have employed the PBE-D2 level of theory to study the direct oxidation of CH_4 to CH_3OH on a Fe–O active site generated on graphene by the decomposition of nitrous oxide (N_2O) over Fe-embedded graphene. Restricted and unrestricted spin state of systems were also taken into account. The calculations show that FeO/graphene provides excellent reactivity for the oxy-functionalization of methane to methanol. The oxygen-centered radicals (O^-) on the catalyst can activate the strong C-H bond of methane leading to its homolytic cleavage. The C-H bond activation requires an energy of 17.5 kcal/mol, which is comparable with the barrier on traditional effective catalysts. Comparing the molecular adsorption complex, the formation of the iron coordinated fragments of C-H activation on the graphene support is found to be less energetically stable than on the Fe sites in the zeolite support. As a result, the conversion of the grafted species to the methanol product in the second step of reaction is much more facile than for Fe-exchanged zeolite catalysts. An activation energy of 16.4 kcal/mol is required to yield the methanol product. Fe–O modified graphene materials could be promising catalysts for the partial oxidation of methane with N_2O as an oxidant.

Introduction

Methane, the major component in natural gas and also a product of fermentation, is one of the useful raw materials for the synthesis of more valuable products such as methanol, formaldehyde, formic acid and also larger hydrocarbons.[1,2] Because the strong tetrahedral C-H bonds of methane (104 kcal/mol),[3] the direct conversion of methane to products is extremely difficult at low temperatures. As a result, a catalyst is needed and the C-H bond activation of methane is considered to be the rate-limiting step in the catalytic partial oxidation of methane. Therefore, over the past few decades many experimental and theoretical investigations[1,2,4-10] have focused on discovering catalysts which can potentially provide not only a high methane conversion rate under mild conditions but also a high selectivity towards the desired product, and to better understand the catalytic processes over metal active sites. In heterogeneous catalysis, optimally accessible metal active sites are needed for the activation of reactants. In order to achieve this, the size of metals becomes one of the most critical factors for the performance of a catalyst. To obtain a fine dispersion of metal, support is needed to prevent aggregation of the metals. Single metal atoms have been anchored on supports such as metal oxides[11-17] and also the inclusion of ion-exchanged metals into porous materials like metal-organic frameworks (MOFs)[18-20] and zeolites has been successful.[11,21-24] Another class of supports, carbonaceous materials such as nanotubes, fullerene and graphene have become promising support materials for metals as well.[25-28] Owing to its high surface area and several unique properties, graphene has extensively been used to investigate many reactions via theoretical and experimental approaches.[25,28-39] The physical and chemical properties of graphene can be tuned by doping alien atoms or nanoparticles. Wang et al.[25] have successfully synthesized metal atom doped graphene using a two-step process. In their work, vacancy sites were firstly created by high-energy atom bombardment and then the desired metals were placed on them. A theoretical study by Krasheninnikov et al.[31] found that the binding of a

[a] Department of Chemistry and NANOTEC Center for Nanoscale Materials Design for Green Nanotechnology, Faculty of Science, Kasetsart University, Bangkok 10900, Thailand

[b] Center for Advanced Studies in Nanotechnology and Its Applications in Chemical, Food and Agricultural Industries, Kasetsart University, Bangkok 10900, Thailand.

[c] PTT Research and Technology Institute, PTT Public Company Limited, Phahonyothin Rd., Sanubtub, Wangnoi, Ayutthaya 13170 Thailand

[d] Institute for Molecular Science and Research Center for Computational Science, Okazaki 444-8585, Japan

[e] PTT Group Frontier Research Center, PTT Public Company Limited, 555 Vibhavadi Rangsit Road, Chatuchak, Bangkok 10900, Thailand

E-mail: jumras.l@ku.ac.th

† Electronic supplementary information (ESI) available. See DOI: 10.1039/b000000x/

metal atom on defective graphene was stronger than on perfect graphene. This finding corresponds well with the work by Wang and coworkers.[25] Therefore, the metal sites might be stable enough as well as might exhibit significant catalytic activity. Recently, we demonstrated theoretically that iron-embedded graphene exhibits good catalytic activity for N_2O decomposition with a low activation energy of 8 kcal/mol.[35] The active Fe–O species is able to oxidize effectively carbon monoxide to carbon dioxide with a low activation barrier. Based on this recent work, it is of interest to look at the product that has been activated from nitrous oxide decomposition with respect to its suitability as the active site for methane activation. The conversion of methane over the FeO/graphene material resembles the catalytic conversion of methane to methanol over the Fe-silicalite zeolites with N_2O as the oxidant.[4,6,8,40-42] The details of the reaction mechanisms and energies and geometrical structures along the catalytic process will be discussed and compared to related systems such as the iron-oxo zeolite mentioned above and bare $[FeO]^+$.

Methodology

In this work, a hexagonal graphene supercell with 4×4 graphene unit cells containing 32 atoms was used as a model. Optimal cell parameters a and b in the graphene plane of 9.91 Å were used.[35] The distance between the graphene sheet and its mirror images was set to 20.0 Å, which is sufficient to exclude the interaction between images.[35] One carbon atom at the center of the graphene sheet was removed to model an atomic vacancy defect. This defect is the simplest one that can occur naturally in all crystalline materials.[32-34] The Fe–O species was incorporated into the model by locating the Fe atom over such a defect point for catalytic study. Spin-restricted and unrestricted periodic DFT calculations were carried out using the DMol[3] code implemented in the Materials Studio package.[43,44] All results were obtained with the Perdew-Burke-Ernzerhof (PBE) functional which belongs to the class of generalized gradient approximation (GGA) functionals.[45] A DN basis with polarization functions (DNP) and the semicore pseudopotentials (DSPPs) were employed for this investigation. In the DSPPs scheme, all electrons are treated explicitly for C, N, O, and H atoms and a relativistic effective potential is used to represent the core electrons of the Fe atom. During the geometry optimization and the transition state (TS) searching steps, the Brillouin zone integration was performed with the Monkhorst-Pack 3×3×1 k-point sampling. The real-space global orbital cutoff radius at fine quality (4.6 Å) and a thermal smearing of 0.005 Hartree (0.136 eV) were used for all calculations. In our calculation, all atoms in the unit cell were allowed to relax. The transition state structures were confirmed to have one imaginary vibrational frequency corresponding to the reaction coordinate. The charge distribution in each system was calculated with the Hirshfeld population analysis.[46] In order to include dispersion interactions, single point calculations with Grimme's method (DFT-D2)[47] were performed. In a recent study,[48] PBE plus Grimme's DFT calculations provided excellent results for geometric, energetic and electronic properties of the graphene/metal interface as compared to experimental data.

Results and discussion

In the previous work mentioned in the introduction,[35] Fe–O deposited on a defective vacancy site of graphene exhibited

catalytic activity to oxidize the CO. In this work, the aim is to investigate its catalytic ability for the C-H bond breaking of methane and the conversion of the dissociated fragment to methanol. Mechanisms for the oxidation of methane to methanol by metal-oxo species have been explored by theoretical and experimental approaches.[1,4-10,41,42] In most cases, the reaction starts with a H abstraction step from methane to the oxo species either via a nonradical or a radical process, leading to the formation of the hydroxyl-grafted metal complex. After the first C-H bond cleavage, the second step is the recombination of two fragments: The –OH and $–CH_3$ moieties form a C-O bond, leading to the formation of the methanol product adsorbed on the metal active center. The spin state has been shown to have an influence on the reaction mechanism. In recent works about catalysis on Fe-based systems,[49-51] the spin inversion has been suggested to play an important role in the catalytic reaction of molecules with the Fe active metal center. Therefore, our investigation considers several spin states of this system.

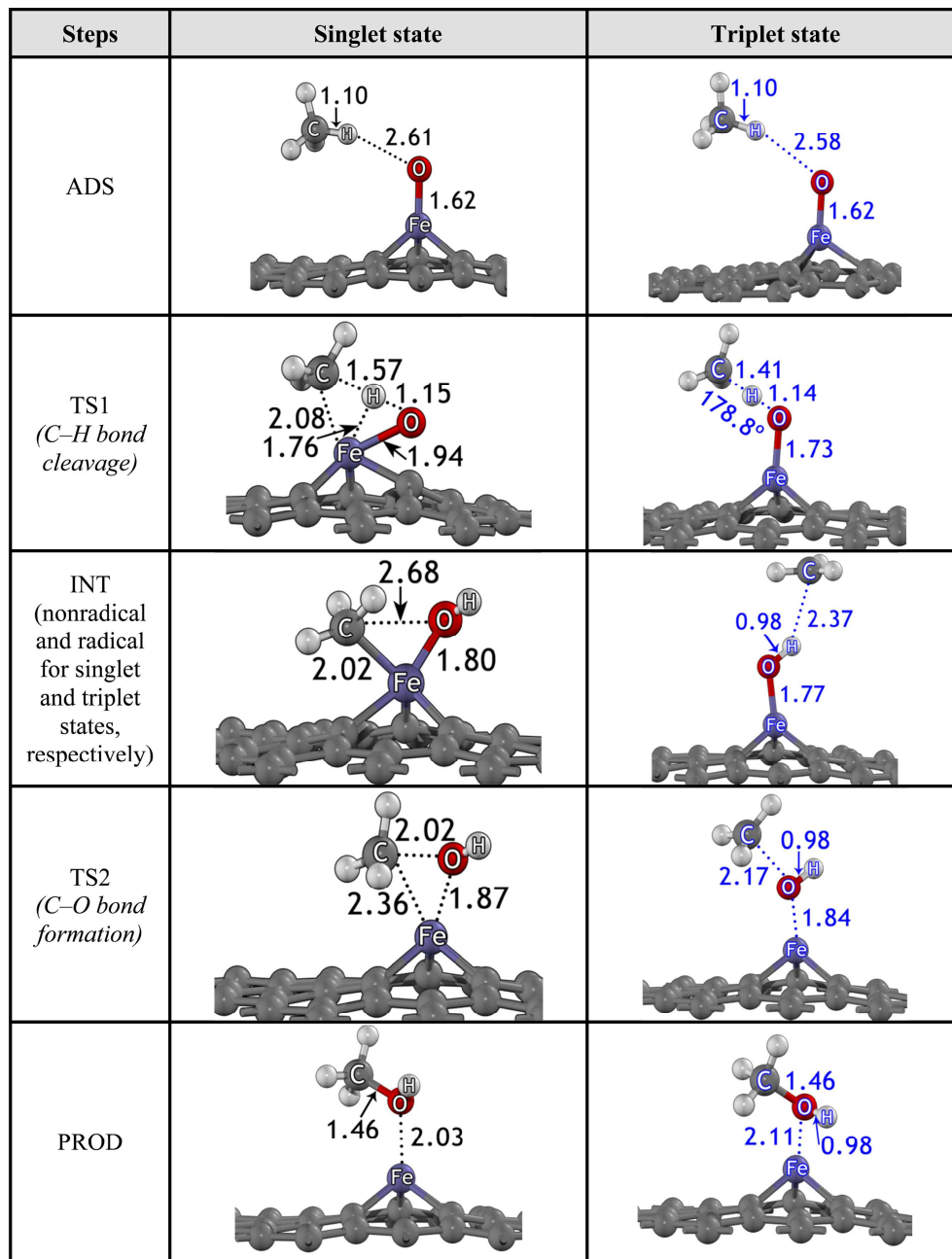### Geometrical structures and electronic properties of Fe–O modified graphene (FeO/graphene)

The optimized structures of the FeO/graphene for singlet and triplet spin states are shown in Fig. S1. All calculations were performed with a fixed spin multiplicity corresponding to the most stable configuration of the initial iron complex. From the calculations, the lowest energy electronic configuration of FeO/graphene can be either the triplet or the singlet spin state. Both are more stable than the quintet spin state by 31.1 kcal/mol. Because of the insignificant difference in the energy of the two lowest spin states (0.1 kcal/mol), spin-crossing between them would play an important role for the relativity of FeO/graphene and the reactivity of FeO/graphene for methane activation was always compared for these two spin states.. The Fe-O bond distances are almost equal too, with a length of 1.615 and 1.619 Å for the singlet and triplet, respectively. This Fe-O bond distance is similar to the bond distance of 1.61-1.65 Å for the Fe-O bond length in the zeolite and in enzyme systems.[7,52-55] The oxygen atom has a negative partial charge of -0.259e and -0.265e (singlet and triplet states, respectively, cf. Table S1 in the Supporting Information). The oxygen deposited on the active iron site protrudes perpendicular from the graphene plane, making it more accessible to incoming adsorbates.

Methane oxidation on the FeO/graphene

The C-H bond activation step

Activation of methane starts with the adsorption of methane on FeO/graphene with one of its hydrogen atoms pointing towards the oxygen atom with an intermolecular distance of about 2.6 Å. The C-H intramolecular distances of methane change only slightly. An electron is transferred from FeO/graphene to methane by 0.033e and 0.035e for the singlet and triplet spin states. As a result, the charge of the carbon atom becomes more negative by 0.016e and the charge of the interacting hydrogen atom becomes less positive by about 0.010e for both spin states. The electron density differences are plotted in Fig. 2. The adsorption energy for both spin states is -2.1 kcal/mol. Comparing with the results for PBE without dispersion correction which are given in the Supporting Information indicate that the adsorption energy is mainly dominated by dispersion interaction. For the singlet spin state, the C-H activation takes place in a nonradical manner. It proceeds

through the four-membered transition state structure associated with hydrogen abstraction from methane to the oxygen atom and, concurrently, the formation of the Fe-C bond (Fig. 1).

| Steps	Singlet state	Triplet state
ADS		
TS1 (C–H bond cleavage)		
INT (nonradical and radical for singlet and triplet states, respectively)		
TS2 (C–O bond formation)		
PROD		

Fig. 1. Optimized structures for the direct oxidation of methane to methanol over FeO/graphene in the singlet and triplet states.

At the transition state of the singlet state spin state, the C-H bond has been elongated from 1.10 to 1.57 Å. At the same state the O-H bond and the Fe-C bond lengths contracted to 1.15 and 2.08 Å, respectively. For the triplet spin state, the C-H cleavage takes place via the radical manner. As a characteristic feature of the direct H-abstraction from methane to the oxygen atom of FeO/graphene an almost linear angle of the C-H-O bond angle (178.8 degrees) can be seen. The C-H bond of methane increased to 1.41 Å and the O-H forming bond is shortened to 1.14 Å. The spin density at the methane moiety increases as shown in Fig. 3. Taking into account the possibility of spin crossing, the C-H bond breaking would take place via the

radical process. The energy barrier for this step is to be 17.5 kcal/mol, which is similar to the energy barrier reported values for various catalysts: FeO$^+$ gas phase (20.1 kcal/mol),[56] the different active forms of the Fe-ZSM-5 zeolite (15-40 kcal/mol),[6-8,57,58] Cu-ZSM-5 zeolite (15.7 kcal/mol),[58] the direct C-H bond activation on the Pt$_{79}$ nanoparticles (7.6 kcal/mol),[60] the surface O$^-$ radical anion of MoO$_3$ (16 kcal/mol)[61] and the MMO enzyme (14-18 kcal/mol),[62] respectively. After this step, the methyl radical and the hydroxo Fe/graphene are formed. The methyl radical has two different ways to proceed. It can bind to the hydroxyl moiety to form the methanol product as shown in the TS_2 profile for the triplet state or it can bind to

the metal active center to form a methyl-hydroxo- Fe/graphene intermediate (CH$_3$-Fe-OH/graphene), "INT_nonradical" in the singlet state profile. The formation of the latter is thermodynamically preferred to the formation of the methyl radical intermediate. As a result, the first half of the hemolytic C-H cleavage would end with the formation of the CH$_3$-Fe-OH/graphene intermediate in the singlet state. The formation of
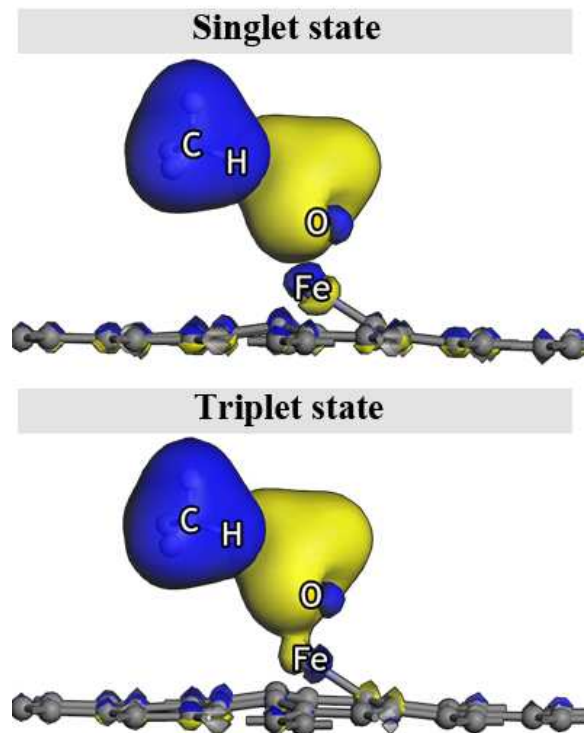

Fig. 2. Electron density difference map calculated from the electron densities of the adsorption state minus its two isolated parts. The isosurface value is ± 0.03 e/Å^3. Regions of electron accumulation/depletion are indicated in blue and yellow colors, respectively

this intermediate is slightly more exothermic than the adsorption complex by 4.4 kcal/mol. One can compare this to the similar case of a FeO species on another support material, Fe-ZSM-5 zeolite, where the direct conversion of methane on the FeO-ZSM-5 was theoretically reported by Yoshizawa et al.[6] The C-H bond activation over the FeO-ZSM-5 leads to the formation of CH$_3$-Fe-OH/ZSM-5 which is much more (22 kcal/mol) stable than the adsorption complex, leading to a very high activation energy of 41.6 kcal/mol for the recombination of ligands to the methanol product in the latter step. At the CH$_3$-Fe-OH/graphene intermediate, the charge of the Fe atom is reduced to 0.175e and the charge of the methyl and hydroxyl moieties have values of -0.014e and -0.131e, respectively. Interestingly, the charge of graphene moiety reversed from positive to negative after the C-H activation (Table S1). The bond between the Fe center and two dissociated fragments are 2.02 and 1.80 Å for the Fe-C and Fe-O bonds, respectively. By thus increasing the coordination number of iron, the geometrical structure between the iron and its surrounding graphene carbon atoms becomes distorted as one of the bonds between iron and graphene carbon is elongated from 1.82 to 1.95 Å. These observations are in agreement with the ones for the C-H bond activation on the oxygen atom of a Fe$_2$O$_3$-like structure,[63] where a homolytic cleavage was taking place.

Methanol formation step

The resulting -CH$_3$ and -OH moieties bound on the Fe center must recombine to methanol, which can occur in the singlet spin state as shown in Fig. 4. At the transition state, two moieties are approaching each other. The bond distances are 2.02 and 1.87 Å for the carbon with its bond to oxygen being formed, and oxygen-iron bond breaks. The transition state for this step is again similar to that for the bare FeO$^+$ complex[42] and for the Fe-ZSM-5 zeolite.[5,6] However, a activation energy of only 16.4 kcal/mol is needed, comparing to the similar process over the Fe-ZSM-5 with an activation energy of 42-53 kcal/mol for CH$_3$-Fe-OH/ZSM-5 zeolite.[5,6] For the Fe-ZSM-5 catalyst, water also needs to be introduced during the methane oxidation reaction in order to increase the rate of methanol formation from the surface methyl intermediates. In that respect, Fe/graphene would have an advantage over Fe-ZSM-5 for this step of the heterogeneously catalyzed methanol formation reaction.
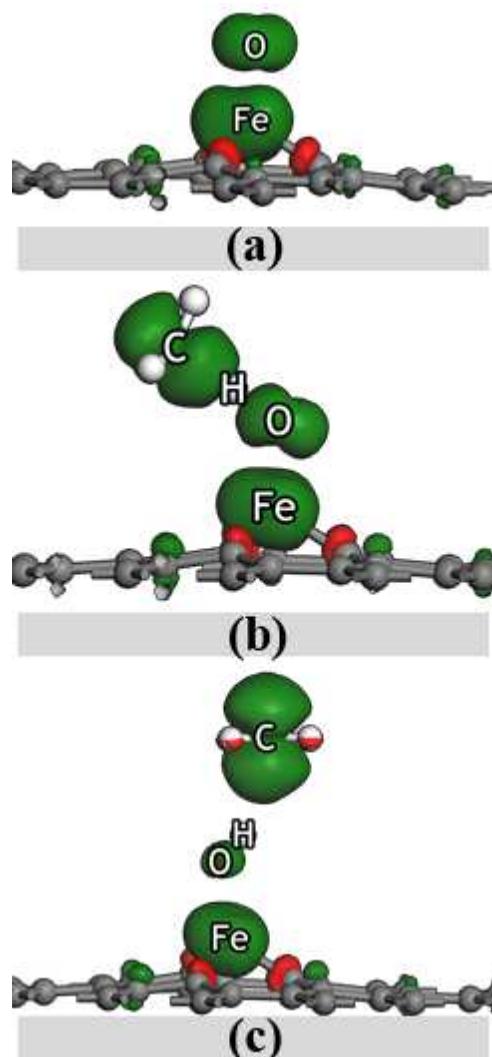

Fig. 3. Spin density distribution for methane activation in the triplet state: (a) ADS, (b) TS and (c) INT_radical complexes. The isosurface value is ± 0.03 e/Å^3. The green isosurface represents α-electron density and the red one represents β-electron density.

The Fe-O distance in the methanol adsorption complex is 2.03 Å and the C-O bond length is 1.46 Å. The adsorption energy of methanol on Fe/graphene is 28.5 kcal/mol, mostly through

lone-pair electron interaction with the metal center. The strong interaction of methanol over the Fe center is similar to the adsorption energy in the Fe-ZSM-5 zeolite (28.8 kcal/mol).[5-7]

As a result, here a solvent is also needed to extract the methanol products from the catalytic centers.
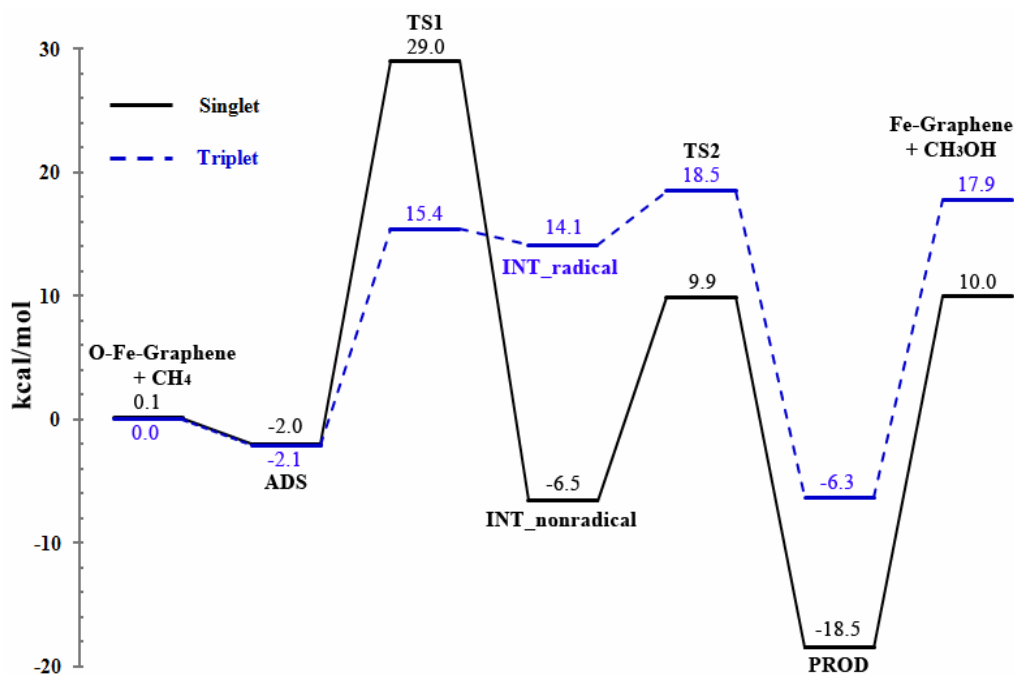
Fig. 4. Energy profile for the direct oxidation of methane to methanol over Fe/O-graphene at the PBE-D2 level of theory. The notation "ADS" and "PROD" refer to the molecular adsorption complex of methane and methanol, respectively. "TS" is the transition state and "INT" the reaction intermediate.

Altogether, however, the results of this work demonstrate an excellent catalytic activity of Fe-graphene as a catalyst for the partial oxidation of methane to methanol. The troublesome conversion of iron hydroxide to the methanol product that occurs in the catalysis using Fe-ZSM-5 zeolite does not occur. After the release of methanol from the metal center, the active oxo species over the iron center can be regenerated through the decomposition of N_2O. Whereas the theoretical results of this study clearly indicate the significant role of the iron-oxo unit deposited on the graphene supporter in the catalytic oxidation of methane to methanol, competitive pathways such as the direct conversion of methane over the Fe-doped graphene or the decomposition of N_2O on the FeO-doped graphene still remain to be thoroughly investigated.

Conclusions

The dispersion-corrected DFT (PBE-D2) was employed to investigate the catalytic conversion of methane to methanol by the FeO/graphene which is generated from the decomposition of N_2O. The catalytic process is divided into two steps. First step is the C-H bond activation process over the oxygen-centered anionic radicals. Through the homolytic cleavage, the C-H bond activation takes place. The activation energy of this step is 17.5 kcal/mol, which is comparable with the values for various catalysts reported for this process. This catalytic process is thermodynamically and kinetically favorable, leading to the hydroxo- methyl- grafted Fe species. This intermediate is expected to be the major species of methane activation rather than the radical intermediate. The methanol product is formed through the recombination of two ligands on iron centers on the

singlet spin state. An activation energy of 16.4 kcal/mol is required in this step. The product desorption from the active site, which requires 28.5 kcal/mol, is the difficult step of the catalytic process.

References

1. H. Schwarz, *Angew. Chem. Int. Ed.*, 2011, **50**, 10096-10115.
2. C. Hammond, S. Conrad and I. Hermans, *ChemSusChem*, 2012, **5**, 1668-1686.
3. S. J. Blanksby and G. B. Ellison, *Acc. Chem. Res.*, 2003, **36**, 255-263.
4. G. I. Panov, V. I. Sobolev, K. A. Dubkov, V. N. Parmon, N. S. Ovanesyan, A. E. Shilov and A. A. Shteinman, *React. Kinet. Catal. Lett.*, 1997, **61**, 251-258.
5. M. F. Fellah and I. Onal, *J. Phys. Chem. C*, 2010, **114**, 3042-3051.
6. K. Yoshizawa, Y. Shiota, T. Yumura and T. Yamabe, *J. Phys. Chem. B*, 2000, **104**, 734-740.

ARTICLE

7. P. Pantu, S. Pabchanda and J. Limtrakul, *Chemphyschem*, 2004, **5**, 1901-1906.
8. W. Liang, A. T. Bell, M. Head-Gordon and A. K. Chakraborty, *J. Phys. Chem. B*, 2004, **108**, 4362-4368.
9. M. H. Baik, M. Newcomb, R. A. Friesner and S. J. Lippard, *Chem. Rev.*, 2003, **103**, 2385-2419.
10. E. V. Starokon, M. V. Parfenov, L. V. Pirutko, S. I. Abornev and G. I. Panov, *J. Phys. Chem. C*, 2011, **115**, 2155-2161.
11. M. Flytzani-Stephanopoulos and B. C. Gates, *Annu. Rev. Chem. Biomol. Eng.*, 2012, **3**, 545-574.
12. A. Uzun, V. Ortalan, Y. Hao, N. D. Browning and B. C. Gates, *J. Phys. Chem. C*, 2009, **113**, 16847-16849.
13. N. Yi, H. Saltsburg and M. Flytzani-Stephanopoulos, *ChemSusChem*, 2013, **6**, 816-819.
14. Z. Zhang, W. Tang, M. Neurock and J. T. Yates, *J. Phys. Chem. C*, 2011, **115**, 23848-23853.
15. W.-J. Chun, Y. Koike, K. Ijima, K. Fujikawa, H. Ashima, M. Nomura, Y. Iwasawa and K. Asakura, *Chem. Phys. Lett.*, 2007, **433**, 345-349.
16. B. Qiao, A. Wang, X. Yang, L. F. Allard, Z. Jiang, Y. Cui, J. Liu, J. Li and T. Zhang, *Nat. Chem.*, 2011, **3**, 634-641.
17. J. L. Gole and M. G. White, *J. Catal.*, 2001, **204**, 249-252.
18. K. L. Mulfort, O. K. Farha, C. L. Stern, A. A. Sarjeant and J. T. Hupp, *J. Am. Chem. Soc.*, 2009, **131**, 3866-3868.
19. D. Himsl, D. Wallacher and M. Hartmann, *Angew. Chem. Int. Ed.*, 2009, **48**, 4639-4642.
20. S. M. Cohen, *Chem. Rev.*, 2012, **112**, 970-1000.
21. P. Kaminski, I. Sobczak, P. Decyk, M. Ziolek, W. J. Roth, B. Campo and M. Daturi, *J. Phys. Chem. C*, 2013, **117**, 2147-2159.
22. W. Gruenert, N. W. Hayes, R. W. Joyner, E. S. Shpiro, M. R. H. Siddiqui and G. N. Baeva, *J. Phys. Chem.*, 1994, **98**, 10832-10846.
23. E. Bayram, J. Lu, C. Aydin, A. Uzun, N. D. Browning, B. C. Gates and R. G. Finke, *ACS Catal.*, 2012, **2**, 1947-1957.
24. S. H. Choi, B. R. Wood, A. T. Bell, M. T. Janicke and K. C. Ott, *J. Phys. Chem. B*, 2004, **108**, 8970-8975.
25. H. Wang, Q. Wang, Y. Cheng, K. Li, Y. Yao, Q. Zhang, C. Dong, P. Wang, U. Schwingenschlogl, W. Yang and X. X. Zhang, *Nano Lett.*, 2012, **12**, 141-144.
26. D. I. Kochubey, V. V. Chesnokov and S. E. Malykhin, *Carbon*, 2012, **50**, 2782-2787.
27. Y. Wang, A. Li, K. Wang, C. Guan, W. Deng, C. Li and X. Wang, *J. Mater. Chem.*, 2010, **20**, 6490.
28. H. Wang, Q. Feng, Y. Cheng, Y. Yao, Q. Wang, K. Li, U. Schwingenschlögl, X. X. Zhang and W. Yang, *J. Phys. Chem. C*, 2013, **117**, 4632-4638.
29. A. K. Geim and K. S. Novoselov, *Nat. Mater.*, 2007, **6**, 183-191.
30. S. Stankovich, D. A. Dikin, G. H. Dommett, K. M. Kohlhaas, E. J. Zimney, E. A. Stach, R. D. Piner, S. T. Nguyen and R. S. Ruoff, *Nature*, 2006, **442**, 282-286.
31. A. V. Krasheninnikov, P. O. Lehtinen, A. S. Foster, P. Pyykko and R. M. Nieminen, *Phys. Rev. Lett.*, 2009, **102**, 126807.
32. M. H. Gass, U. Bangert, A. L. Bleloch, P. Wang, R. R. Nair and A. K. Geim, *Nat. Nanotechnol.*, 2008, **3**, 676-681.
33. M. M. Ugeda, I. Brihuega, F. Guinea and J. M. Gomez-Rodriguez, *Phys. Rev. Lett.*, 2010, **104**, 096804.
34. J. C. Meyer, C. Kisielowski, R. Erni, M. D. Rossell, M. F. Crommie and A. Zettl, *Nano. Lett.*, 2008, **8**, 3582-3586.
35. S. Wannakao, T. Nongnual, P. Khongpracha, T. Maihom and J. Limtrakul, *J. Phys. Chem. C*, 2012, **116**, 16992-16998.
36. P. Janthon, F. Vines, S. M. Kozlov, J. Limtrakul and F. Illas, *J. Chem. Phys.*, 2013, **138**, 244701.
37. H. Vovusha, S. Sanyal and B. Sanyal, *J. Phys. Chem. Lett.*, 2013, **4**, 3710-3718.
38. J. K. Wassei and R. B. Kaner, *Acc. Chem. Res.*, 2013, **46**, 2244–2253.
39. X. F. Yang, A. Wang, B. Qiao, J. Li, J. Liu and T. Zhang, *Acc. Chem. Res.*, 2013, **46**, 1740-1748.
40. G. I. Panov, A. K. Uriarte, M. A. Rodkin and V. I. Sobolev, *Catal. Today*, 1998, **41**, 365-385.
41. B. R. Wood, J. A. Reimer, A. T. Bell, M. T. Janicke and K. C. Ott, *J. Catal.*, 2004, **225**, 300-306.
42. K. Yoshizawa, *Acc. Chem. Res.*, 2006, **39**, 375-382.
43. B. Delley, *J. Chem. Phys.*, 1990, **92**, 508.
44. B. Delley, *J. Chem. Phys.*, 2000, **113**, 7756.
45. J. P. Perdew, K. Burke and M. Ernzerhof, *Phys. Rev. Lett.*, 1996, **77**, 3865-3868.
46. F. L. Hirshfeld, *Theor. Chim. Acta*, 1977, **44**, 129-138.
47. S. Grimme, *J. Comput. Chem.*, 2006, **27**, 1787-1799.
48. P. Janthon, F. Viñes, S. M. Kozlov, J. Limtrtakul and F. Illas, *J. Chem. Phys.*, 2013, **138**, 244701-244708.
49. A. Jedidi, W. Norelus, A. Markovits, C. Minot, F. Illas and M. Abderrabba, *Theor. Chem. Acc.*, 2014, **133**, 1430-1440.
50. Z. Liu, W. Guo, L. Zhao and H. Shan, *J. Phys. Chem. A*, 2010, **114**, 2701-2709.
51. X.-L. Sun, X.-R. Huang, J.-L. Li, R.-P. Huo and C.-C. Sun, *J. Phys. Chem. A*, 2012, **116,** 1475-1485.
52. I. Schlichting, *Science*, 2000, **287**, 1615-1622.
53. J. Sirijaraensre and J. Limtrakul, *Struct. Chem.*, 2012, **24**, 1307-1318.
54. T. Maihom, P. Khongpracha, J. Sirijaraensre and J. Limtrakul, *Chemphyschem*, 2013, **14**, 101-107.
55. G. Li, E. A. Pidko, R. A. van Santen, Z. Feng, C. Li and E. J. M. Hensen, *J. Catal.*, 2011, **284**, 194-206.
56. G. Altinay, M. Citir and R. B. Metz, *J. Phys. Chem. A*, 2010, **114**, 5104-5112.
57. M. F. Fellah and I. Onal, *J. Phys. Chem. C*, 2012, **116**, 13616-13622.
58. M. F. Fellah, *J. Catal.*, 2011, **282**, 191-200.
59. J. S. Woertink, P. J. Smeets, M. H. Groothaert, M. A. Vance, B. F. Sels, R. A. Schoonheydt and E. I. Solomon, *Proc. Natl. Acad. Sci.*, 2009, **106**, 18908-18913.
60. F. Viñes, Y. Lykhach, T. Staudt, M. P. A. Lorenz, C. Papp, H.-P. Steinrück, J. Libuda, K. M. Neyman and A. Görling, *Chem. Eur. J.*, 2010, **16**, 6530-6539.
61. S. P. Mehandru, A. B. Anderson, J. F. Brazdil and R. K. Grasselli, *J. Phys. Chem.*, 1987, **91**, 2930-2934.
62. A. M. Valentine, S. S. Stahl and S. J. Lippard, *J. Am. Chem. Soc.*, 1999, **121**, 3876-3887.
63. S. Motozuka, M. Tagaya, T. Ikoma, M. Morinaga, T. Yoshioka and J. Tanaka, *J. Phys. Chem. C*, 2013, **117**, 16104-16118.
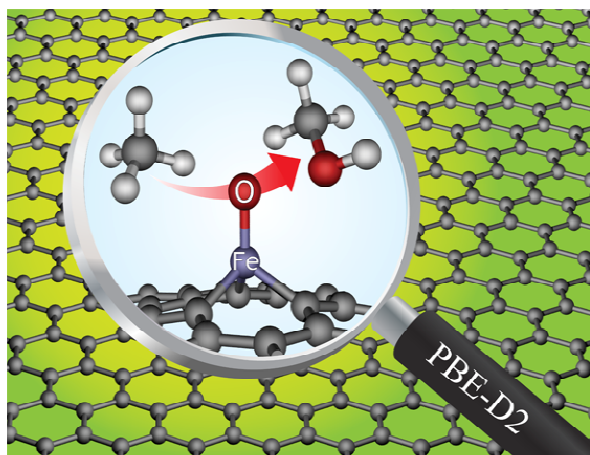
The reaction mechanisms and energetic profiles of the partial oxidation of methane to methanol over the FeO-unit deposited graphene have been theoretically investigated by means of the PBE functional with Grimme's dispersion correction (PBE-D2).